Journal of Clinical and Translational Hepatology **2026**
DOI: 10.14218/JCTH.2026.00278

Original Article

Single-cell RNA Sequencing Analysis Reveals That Targeting PLG–PLGRKT Signaling-mediated Pro-fibrotic Scar-associated Macrophages Ameliorates Liver Fibrosis in Biliary Atresia

Xin Li[1,2#], Tengfei Li[2,3#], Shaowen Liu[2,3#], Qianhui Yang[2,3], Yuqiang Chen[1,2], Yu Meng[2,3], Xiaodan Xu[2,3], Yilin Zhao[2,3], Yanran Zhang[2,3], Jiaying Liu[2,3], Rongjuan Sun[2,3] and Alimujiang Abudureyimu[1*]

[1]Department of General Surgery, Urumqi Children's Hospital, Urumqi, Xinjiang, China; [2]Graduate School, Tianjin Medical University, Tianjin, China; [3]Department of General Surgery, Tianjin Children's Hospital, Tianjin, China

Received: April 09, 2026 | **Revised:** June 11, 2026 | **Accepted:** August 27, 2026 | **Published online:** September 09, 2026

Abstract

Background and Aims: Biliary atresia (BA) is a severe pediatric cholangiopathy characterized by rapidly progressive liver fibrosis. This study aimed to characterize scar-associated macrophages and investigate the role of PLG–PLGRKT signaling in BA-associated fibrogenesis. ***Methods:*** Single-cell RNA sequencing and spatial transcriptomics were applied to liver tissues from patients with BA and non-BA controls. Key findings were validated in an independent cohort using quantitative polymerase chain reaction and multiplex immunohistochemistry. The functional role of the PLGRKT pathway was further examined using primary human peripheral blood mononuclear cell-derived macrophages with small interfering RNA (siRNA)-mediated PLGRKT knockdown, together with co-culture systems involving LX-2 hepatic stellate cells and human liver organoids. In vivo therapeutic potential was evaluated in a murine bile duct ligation model of cholestatic liver fibrosis using macrophage-targeted Plgrkt–Trem2 antibody–siRNA conjugates. ***Results:*** In BA, scar-associated macrophages (SAMs) increased with fibrosis progression and co-localized with hepatic stellate cells in fibrotic areas. PLGRKT was upregulated in BA liver tissue and increased during monocyte-to-macrophage differentiation. In primary human macrophages, plasminogen induced a PLGRKT-dependent pro-fibrotic phenotype, and conditioned medium from these cells increased COL1A1 deposition in hepatic stellate cells and human liver organoids. In vivo, macrophage-targeted Plgrkt–Trem2 antibody–siRNA conjugates reduced SAM accumulation and attenuated bile duct ligation-induced liver fibrosis. ***Conclusions:*** These findings support a role for SAMs and the PLGRKT–SAM axis in BA-associated liver fibrosis and suggest that PLGRKT warrants further investigation as a potential macrophage-directed anti-fibrotic target.

Keywords: Biliary atresia; Liver fibrosis; Liver organoids; PLGRKT; Scar-associated macrophages; scRNA-seq.

[#]Contributed equally to this work.

[*]**Correspondence to:** Alimujiang Abudureyimu, Department of General Surgery, Urumqi Children's Hospital, Urumqi, Xinjiang 830000, China. ORCID: https://orcid.org/0000-0001-7680-322X. Tel: +86-186-9919-6954, E-mail: alimujiang_wlmq@163.com.

Citation of this article: Li X, Li T, Liu S, Yang Q, Chen Y, Meng Y, *et al*. Single-cell RNA Sequencing Analysis Reveals That Targeting PLG–PLGRKT Signaling-mediated Pro-fibrotic Scar-associated Macrophages Ameliorates Liver Fibrosis in Biliary Atresia. J Clin Transl Hepatol 2026. doi: 10.14218/JCTH.2026.00278.

Introduction

Biliary atresia (BA) is a severe and progressive inflammatory cholangiopathy unique to neonates and infants, characterized by fibro-obliteration of the extrahepatic and intrahepatic bile ducts. This obstruction leads to cholestasis and subsequent severe liver fibrosis, which can progress rapidly.[1,2] Despite early surgical intervention with Kasai portoenterostomy, most patients ultimately develop end-stage liver disease and cirrhosis, making BA the leading indication for pediatric liver transplantation worldwide.[1,3,4] The aggressive clinical course of BA highlights an urgent need for targeted anti-fibrotic therapies. Its rapid fibrogenesis suggests that distinct cellular and molecular drivers within the pediatric liver microenvironment may differ from those in adult chronic liver diseases.

Hepatic stellate cells (HSCs) are widely recognized as principal mediators of liver fibrosis. Following chronic liver injury, quiescent HSCs transdifferentiate into activated myofibroblasts that synthesize and deposit excessive extracellular matrix proteins, leading to scar formation and progressive organ dysfunction.[5,6] This activation is not cell autonomous but is driven by intercellular crosstalk within the liver microenvironment, where immune cells—particularly macrophages—play key roles in regulating HSC activation and fibrogenesis.[7–10]

Advances in single-cell RNA sequencing (scRNA-seq) have improved our understanding of macrophage heterogeneity and plasticity in fibrotic diseases of multiple organs, including the liver, lung, kidney, and heart.[11–19] In our previous study, infiltration of scar-associated macrophages (SAMs) increased in BA livers and was associated with fibrosis progression.[20] SAMs are characterized by expression of a core

Copyright: © 2026 The Author(s). This article has been published under the terms of Creative Commons Attribution-Noncommercial 4.0 International License (CC BY-NC 4.0), which permits noncommercial unrestricted use, distribution, and reproduction in any medium, provided that the following statement is provided. "This article has been published in *Journal of Clinical and Translational Hepatology* at https://doi.org/10.14218/JCTH.2026.00278 and can also be viewed on the Journal's website at http://www.jcthnet.com".

set of markers, including TREM2, CD9, SPP1, GPNMB, and LGALS3.[9,11,21–23] These cells are predominantly derived from recruited circulating monocytes and localize within the "fibrotic niche," the microanatomical region of active scarring in cirrhotic human liver tissue and various murine models of liver fibrosis.[11,22,24] Within this niche, SAMs interact with HSCs and other stromal cells and may contribute to fibrosis progression.[9,11,22] Although immune dysregulation and macrophage involvement are recognized features of BA,[25] the specific contribution, phenotypic identity, and molecular regulation of SAMs in the rapidly fibrosing BA liver remain incompletely defined.

Although SAMs have emerged as important mediators of fibrogenesis in several chronic liver diseases, their precise role in BA remains incompletely understood. The plasminogen receptor with a C-terminal lysine (PLGRKT; Plg-RKT in mice) is a transmembrane receptor with both N- and C-termini exposed extracellularly and is predominantly expressed on myeloid cells such as monocytes and macrophages.[26,27] PLGRKT binds plasminogen (PLG) and enhances its activation to plasmin at the cell surface, facilitating pericellular proteolysis, cell migration, and phenotypic changes.[28] Foundational work in murine models of liver fibrosis showed that SAMs highly express Plg-RKT and that the PLG–PLGRKT signaling axis is involved in monocyte differentiation into pro-fibrotic SAMs.[12] However, whether PLGRKT-mediated SAM differentiation contributes to fibrosis progression and represents a potential therapeutic target in BA remains unknown.

We hypothesized that PLGRKT promotes the differentiation and pro-fibrotic activity of SAMs, thereby contributing to liver fibrosis progression in BA. To test this hypothesis, we integrated scRNA-seq and spatial transcriptomics analyses of BA liver tissues with validation in independent patient cohorts. We then examined the functional role of PLGRKT in SAM differentiation and pro-fibrotic activity using *in vitro* macrophage and co-culture models and assessed its therapeutic potential in a murine bile duct ligation (BDL) model. Together, these approaches were designed to evaluate the PLGRKT–SAM axis as a potential mediator and therapeutic target in BA-associated liver fibrosis.

Methods

Study design and sample collection

This study aimed to characterize SAMs in BA-associated liver fibrosis, investigate the role of PLG–PLGRKT signaling in pro-fibrotic SAM differentiation and SAM–HSC interactions, and evaluate a TREM2 antibody–siRNA conjugate for targeted gene silencing in SAMs. Liver tissue specimens were collected from pediatric patients undergoing surgery at Urumqi Children's Hospital between December 2023 and December 2024 (Supplementary Table 1).[20] Initial omics analyses (scRNA-seq and spatial transcriptomics) included liver tissues from four patients with type III BA and four age-matched non-fibrotic disease controls (DC). The DC group comprised liver tissues from two children with choledochal cysts, designated as choledochal cyst controls (CC), and peritumoral liver tissues from one child with hepatic hemangioma and one child with hepatoblastoma, designated as normal controls (NC).[29] An expanded independent validation cohort comprised 20 patients with BA and 10 DC. Liver fibrosis was staged by two blinded pathologists according to the METAVIR system.[30] Clinical and demographic data are detailed in Supplementary Table 2. The study was approved by the Ethics Committee of Urumqi Children's Hospital (K2024-04), conducted in accordance with the Declaration of Helsinki (as revised in 2024), and written informed consent was obtained from the legal guardians. Animal experiments were additionally approved by the relevant ethics committee (approval no. GENINK-20250194).

Single-cell RNA sequencing processing and analysis

To identify cell type-specific transcriptomic alterations in BA livers, we performed scRNA-seq on freshly collected liver tissues. Libraries were prepared using the Singleron GEXSCOPE platform (Singleron Biotechnologies, Nanjing, Jiangsu, China) according to the manufacturer's protocol. Sequencing was performed on a NovaSeq 6000 platform (Illumina, San Diego, CA, USA). Data were processed using Seurat (v4.1.1).[31] Potential doublets were removed using DoubletFinder (v2.0.3),[32] and cells were filtered using standard quality-control criteria (nFeature_RNA ≥ 200, nCount_RNA ≥ 500, log10FeaturePerUMI ≥ 0.8, percent_mito ≤ 15%). Data normalization, variance stabilization, and batch-effect correction were performed using SCTransform.[33] Principal component analysis was used for dimensionality reduction, and the first 30 principal components were used for graph-based clustering with the shared nearest-neighbor algorithm (resolution, 0.5 for initial broad cell type identification).[33] Cell types were annotated based on canonical marker-gene expression. Differentially expressed genes between clusters were identified using the Wilcoxon rank-sum test with Benjamini–Hochberg false-discovery rate correction (FDR < 0.05; |logFC| > 0.25; expression prevalence ≥ 10%).[34] Gene Ontology and Kyoto Encyclopedia of Genes and Genomes pathway enrichment analyses were performed using clusterProfiler (v4.6.2).[35] Pseudotemporal trajectory analysis was conducted using Monocle,[36] and cell–cell communication networks were inferred using CellChat (v1.5.0).[37]

Spatial transcriptomics processing and analysis

To determine the spatial localization of cell populations identified by scRNA-seq, we performed spatial transcriptomics on formalin-fixed, paraffin-embedded (FFPE) liver sections. Spatial transcriptomics experiments were performed using the 10x Genomics Visium platform with CytAssist (10x Genomics, Pleasanton, CA, USA), as previously described.[38] Briefly, 5 μm-thick sections were cut from FFPE liver tissue blocks and stained with hematoxylin and eosin (H&E).[39] Target probes were hybridized to selected tissue regions, and sections were transferred onto Visium Spatial Gene Expression slides using the CytAssist instrument. Spatial transcriptomics image enhancement was performed using BayesSpace.[40] Marker-gene enrichment scores for each major cell type were calculated for each spatial transcriptomics spot using AUCell,[41] and multigene co-expression patterns were visualized using SpatialFeaturePlot.

Histopathology and immunohistochemistry

To validate key fibrosis-associated markers at the protein level, we performed histopathological staining and immunohistochemistry (IHC) on liver sections. FFPE liver tissues were fixed in 4% paraformaldehyde, embedded in paraffin, and sectioned at 4 μm. H&E staining was performed according to standard protocols.[39] IHC was performed as previously described.[42] Briefly, sections were deparaffinized, rehydrated, subjected to heat-induced antigen retrieval (EDTA, pH 9.0), and blocked for endogenous peroxidase activity and nonspecific serum binding. Primary antibodies were incubated overnight at 4°C: CD9 (Proteintech, 60232-1-g; Rosemont, IL, USA; 1:200), TREM2 (Abcam, ab223684; Cambridge, UK; 1:250), and PLG-RKT (Thermo Fisher Scientific, PA5-98932;

Waltham, MA, USA; 1:100) (Supplementary Table 3). Detection was performed with horseradish peroxidase-conjugated secondary antibodies and 3,3′-diaminobenzidine substrate, followed by hematoxylin counterstaining. The immunopositive area (%) was quantified using ImageJ (v1.53; NIH, Bethesda, MD, USA), as previously described.[43] Liver fibrosis was assessed by Sirius Red staining, as previously described.[44]

Multiplex immunofluorescence

To visualize spatial relationships among macrophage subsets, activated hepatic stellate cells, and fibrosis markers, we performed multiplex immunofluorescence on liver tissue sections using a Multiplex Fluorescence Staining Kit (DK750; Biomark Biology, Nanjing, Jiangsu, China) according to the manufacturer's instructions, as previously described.[45] The following primary antibodies were used: alpha-smooth muscle actin (α-SMA; CST, 19245S; Cell Signaling Technology, Danvers, MA, USA; 1:600), CD68 (Abcam, ab213363; Cambridge, UK; 1:1,000), TREM2 (Abcam, ab223684; Cambridge, UK; 1:250), CD9 (Proteintech, 60232-1-g; Rosemont, IL, USA; 1:200), PLG-RKT (Thermo Fisher Scientific, PA5-98932; Waltham, MA, USA; 1:100), LGALS1 (Abcam, ab138513; Cambridge, UK; 1:10,000), SPP1 (Abcam, ab283656; Cambridge, UK; 1:2,000), LGALS3 (Abcam, ab76245; Cambridge, UK; 1:250), GPNMB (Abcam, ab222109; Cambridge, UK; 1:1,000), and ANXA2 (Abcam, ab178627; Cambridge, UK; 1:100)(Supplementary Table 4). Nuclei were counterstained with 4′,6-diamidino-2-phenylindole (DAPI). Whole-slide images were acquired using TissueFAXS (TissueGnostics, Vienna, Austria) and analyzed in StrataQuest (TissueGnostics) for cell-phenotype identification, marker-intensity quantification, and spatial-metric analysis.

Reverse transcription quantitative polymerase chain reaction analysis

To quantify gene-expression changes in liver tissues and cultured macrophages, we performed reverse transcription quantitative polymerase chain reaction (RT-qPCR). Total RNA was extracted from frozen human liver tissue and *in vitro*-cultured human macrophages using the EasyPure Fast Cell RNA Kit (TransGen Biotech, ER111-02; Beijing, China) and from mouse liver using Superbrilliant TRI RNA (ZS-M11008; Zhongshi Gene Technology, Tianjin, China). RNA concentration was measured using a NanoDrop One spectrophotometer (Thermo Fisher Scientific, Waltham, MA, USA).[46] cDNA synthesis and quantitative PCR were performed with TransScript Green One-Step qRT-PCR SuperMix (TransGen Biotech, AQ211-02; Beijing, China) on a QuantStudio 7 Pro Real-Time PCR System (Applied Biosystems/Thermo Fisher Scientific, Waltham, MA, USA); for mouse samples, first-strand cDNA was generated using the Supersmart 6-min Heat-Resistant First-Strand cDNA Synthesis Kit (ZS-M14003; Zhongshi Gene Technology, Tianjin, China). Relative mRNA expression was calculated using the $2^{-\Delta\Delta Ct}$ method,[47] normalized to *GAPDH* (human) or *Actb* (mouse). Primer sequences are listed in Supplementary Tables 5 (human) and 6 (mouse).

siRNA–TREM2 antibody conjugates

To enable targeted gene knockdown in SAMs, we synthesized TREM2 antibody–siRNA conjugates. siRNA targeting mouse *Plgrkt* was chemically conjugated to a purified anti-mouse TREM2 antibody (BioLegend, 824804; San Diego, CA, USA) using a cleavable disulfide linker, as previously described.[48] A negative-control siRNA sequence was conjugated to the same TREM2 antibody; conjugates were synthesized and purified by Zhongshi Gene Technology (Tianjin, China). Conjugation efficiency was verified by high-performance liquid chromatography, as previously described.[48]

Preliminary uptake and distribution assays

To confirm cellular uptake of the conjugates by macrophages, we performed *in vitro* and *in vivo* distribution assays. For *in vitro* uptake, RAW264.7 macrophages (ATCC, Manassas, VA, USA) were seeded onto coverslips, incubated overnight, and exposed to Cy5-labeled TREM2–siRNA conjugates for 2 h. Cells were fixed with 4% paraformaldehyde, mounted in DAPI-containing mounting medium, and examined by fluorescence microscopy, as previously described.[48] For *in vivo* distribution, Cy5-labeled TREM2–siRNA conjugates (4.0 mg/kg) were injected via the tail vein. After 2 h, mice were sacrificed, and livers were excised, embedded in optimal cutting temperature compound, cryosectioned, and stained with F4/80-Cy3. Co-localization of conjugates with F4/80+ macrophages was assessed by fluorescence microscopy (Akoya Biosciences, Marlborough, MA, USA).[48]

Animal model and in vivo siRNA treatment

To evaluate the therapeutic efficacy of TREM2–siRNA conjugates *in vivo*, we used a bile duct ligation (BDL) mouse model of obstructive cholestasis and liver fibrosis. Male BALB/c mice (6–8 weeks old; 20–25 g) were housed under specific pathogen-free conditions with a 12 h light/dark cycle and ad libitum access to food and water. All procedures were approved by the Animal Ethics Committee of Tianjin Medical University. BDL was performed as previously described.[49] Briefly, under isoflurane anesthesia, the common bile duct was isolated, double-ligated, and transected; sham-operated mice underwent the same procedure without ligation. Mice (n = 5 per group) were randomly assigned to four groups: (1) sham + vehicle (saline), (2) BDL + vehicle, (3) BDL + negative-control TREM2–siRNA conjugate, and (4) BDL + *Plgrkt*–TREM2–siRNA conjugate. Conjugates (4.0 mg/kg) or saline were administered via tail-vein injection beginning 1 day after surgery and then every other day for 14 days. Mice were monitored daily; on day 14, they were sacrificed under deep anesthesia, and blood and liver tissues were collected for downstream analyses.

Human peripheral blood mononuclear cell isolation and macrophage differentiation

To obtain primary human macrophages for in vitro functional assays, we isolated peripheral blood mononuclear cells (PBMCs) from healthy donors and differentiated them into macrophages. Human PBMCs were isolated from healthy-donor buffy coats by density-gradient centrifugation using Lymphocyte Separation Medium, as previously described.[50] For macrophage differentiation, thawed PBMCs were seeded at 7×10^5 cells/well in 12-well plates and cultured in RPMI 1640 supplemented with GlutaMAX, HEPES, 10% fetal bovine serum (Gibco/Thermo Fisher Scientific, Grand Island, NY, USA), M-CSF (50 ng/mL; R&D Systems, Minneapolis, MN, USA), and IL-4 (20 ng/mL; R&D Systems) for 6–7 days, as previously described.[51]

Induction of SAM phenotype and siRNA transfection

To investigate the functional role of PLG-RKT signaling in SAM polarization, we induced a SAM-like phenotype in differentiated human macrophages *in vitro*. Macrophages were stimulated with plasminogen (PLG; 4 μg/mL; Roche, 10874477001; Basel, Switzerland) for 6 h, as previously described.[12] For PLGRKT knockdown experiments, macrophages were transfected with 20 pmol of siRNA targeting PLGRKT (siPLGRKT)

or negative-control siRNA (siNC) using LipORNAi transfection reagent (Beyotime, C0535; Shanghai, China) according to the manufacturer's protocol,[52] 48 h before PLG stimulation.

Cell culture and liver organoid generation

To model cellular interactions involved in BA-associated liver fibrosis *in vitro*, we established a THLE-2/LX-2 liver organoid system. THLE-2 cells were cultured in Liver Organoid Growth Medium (AcroGenic, AC0217; Beijing, China).[53] LX-2 human hepatic stellate cells (MilliporeSigma, Burlington, MA, USA) were cultured in DMEM (Gibco, C11965500BT; Grand Island, NY, USA) with 10% fetal bovine serum. Liver organoids were generated by mixing THLE-2 and LX-2 cells at a 3:1 ratio (total, 2×10^5 cells per 100 μL) with 50 μL of Liver Organoid Matrix (AcroGenic, AC0217; Beijing, China), as previously described.[54–56] The mixture was seeded into ultra-low-attachment 96-well plates (Corning, Corning, NY, USA) and cultured in Liver Organoid Complete Growth Medium for 2–3 weeks, with half-medium changes every 2–3 days. Organoids with diameters of approximately 150 μm were used for subsequent experiments.

Conditioned medium experiments

To assess the paracrine effects of SAM-secreted factors on hepatic stellate cells and liver organoids, we performed conditioned-medium (CM) transfer experiments. Macrophages were treated with PLG (4 μg/mL) or vehicle control as described above. For knockdown experiments, macrophages were transfected with siPLGRKT or siNC 48 h before PLG stimulation. After 6 h of PLG stimulation, culture supernatants were collected, centrifuged (3,000 × g, 10 min, 4°C) to remove cellular debris, and stored at −80°C. LX-2 cells or liver organoids were cultured in medium containing 50% CM for 96 h (LX-2 cells) or 3–4 days (organoids).[57]

Flow cytometry

To quantify SAM-marker expression in human macrophages and mouse liver non-parenchymal cells, we performed flow cytometry. Human macrophages were washed in phosphate-buffered saline and stained for 30 min at 4°C in the dark with human TREM2-APC (R&D Systems, FAB17291A; Minneapolis, MN, USA) and human CD9-Alexa Fluor 488 (R&D Systems, FAB1880G) or isotype controls and then analyzed on a CytoFLEX LX (Beckman Coulter, Brea, CA, USA); data were processed in FlowJo (v10.0; BD Biosciences, Ashland, OR, USA).[58] For mouse liver, non-parenchymal cells were isolated by collagenase IV perfusion/digestion and Percoll density separation followed by red blood cell lysis, as previously described.[59] Non-parenchymal cells (1×10^6 cells) were Fc-blocked with TruStain FcX (BioLegend, San Diego, CA, USA) and stained with CD45 PE/Cy7 (BioLegend, 103113), F4/80 PerCP/Cy5.5 (Elabscience, E-AB-F0995UJ; Houston, TX, USA), TREM2 PE (BioLegend, 824805), CD9 APC (BioLegend, 124811), and Ly6G BV421 (BioLegend, 127627)(Supplementary Table 7). Cells were acquired on a BD FACSVerse (BD Biosciences, San Jose, CA, USA) and analyzed in FlowJo v10.0. SAMs were defined as singlet, live, CD45+ Ly6G− F4/80+ TREM2+ CD9+ cells.

Immunofluorescence analysis

To examine the expression and co-localization of PLG-RKT and collagen in macrophages and organoids, we performed immunofluorescence staining. Cells on coverslips were fixed in 4% paraformaldehyde (30 min), permeabilized with 0.1% Triton X-100, and blocked with 10% goat serum (Beyotime, C0265; Shanghai, China). Primary antibodies—anti-PLG-RKT (Invitrogen/Thermo Fisher Scientific, PA5-98932; Waltham, MA, USA) and anti-COL1A1 (CST, 66948S; Danvers, MA, USA)—were applied overnight at 4°C, followed by Alexa Fluor-conjugated secondary antibodies (CST, 4408S and 4413S; Danvers, MA, USA) for 2 h at room temperature; nuclei were counterstained with DAPI (CST, 4083S). Images were acquired on an EVOS M5000 (Invitrogen/Thermo Fisher Scientific, Waltham, MA, USA). Organoid samples were fixed in 4% paraformaldehyde (6 h); the matrix was digested with cellulase (Sigma-Aldrich, C2730; St. Louis, MO, USA) in 2 mM EDTA/phosphate-buffered saline, and samples were then permeabilized, blocked, and stained as described above.[54,55]

Western blot analysis

To assess protein-level changes in signaling pathways and fibrosis markers, we performed Western blotting. Proteins were extracted using RIPA lysis buffer (Beyotime, Shanghai, China) supplemented with protease-inhibitor cocktail (Roche, Basel, Switzerland), quantified by BCA assay (Pierce/Thermo Fisher Scientific, Waltham, MA, USA), separated by SDS-PAGE, and transferred to PVDF membranes (MilliporeSigma, Burlington, MA, USA), as previously described.[60] Membranes were blocked in 5% nonfat milk or bovine serum albumin, incubated overnight at 4°C with the primary antibodies listed in Supplementary Table 8, and detected with horseradish peroxidase-conjugated secondary antibodies. Protein signals were visualized by enhanced chemiluminescence and quantified using ImageJ (v1.53; NIH, Bethesda, MD, USA).[43]

Liver function tests

To evaluate liver injury in the BDL mouse model, we measured serum biochemical markers. Serum alanine aminotransferase (ALT), aspartate aminotransferase (AST), alkaline phosphatase (ALP), gamma-glutamyl transferase (GGT), total bilirubin (TBIL), direct bilirubin (DBIL), and total bile acids (TBA) were measured using an automated biochemical analyzer (Hitachi, Tokyo, Japan), as previously described.[49] The AST-to-platelet ratio index was calculated as previously reported.[61]

Statistical analysis

Statistical analyses were performed using R (v4.1.3; R Foundation for Statistical Computing, Vienna, Austria). Data visualization was performed using the ggplot2 package. Image processing and quantification were performed using ImageJ (v1.53; NIH, Bethesda, MD, USA).[43] Two-group comparisons were performed using the unpaired two-tailed Student *t* test or Mann–Whitney U test, depending on data distribution and variance. Multiple-group comparisons were conducted using one-way analysis of variance with the Tukey post hoc test or Kruskal–Wallis test with the Dunn post hoc test. Proportions were compared using the chi-square test or Fisher exact test, and correlations were assessed using Pearson or Spearman correlation coefficients. *P* values were adjusted for multiple comparisons using the Benjamini–Hochberg method where appropriate. A P value < 0.05 was considered statistically significant. Data are presented as mean ± standard deviation or median (interquartile range), as appropriate.

Results

Single-cell RNA sequencing analysis identified SAM enrichment associated with BA liver fibrosis

scRNA-seq analysis of liver tissues from patients with BA and DC identified 10 major cell populations in the hepatic microenvironment, including T/NK cells, B cells, monocyte–

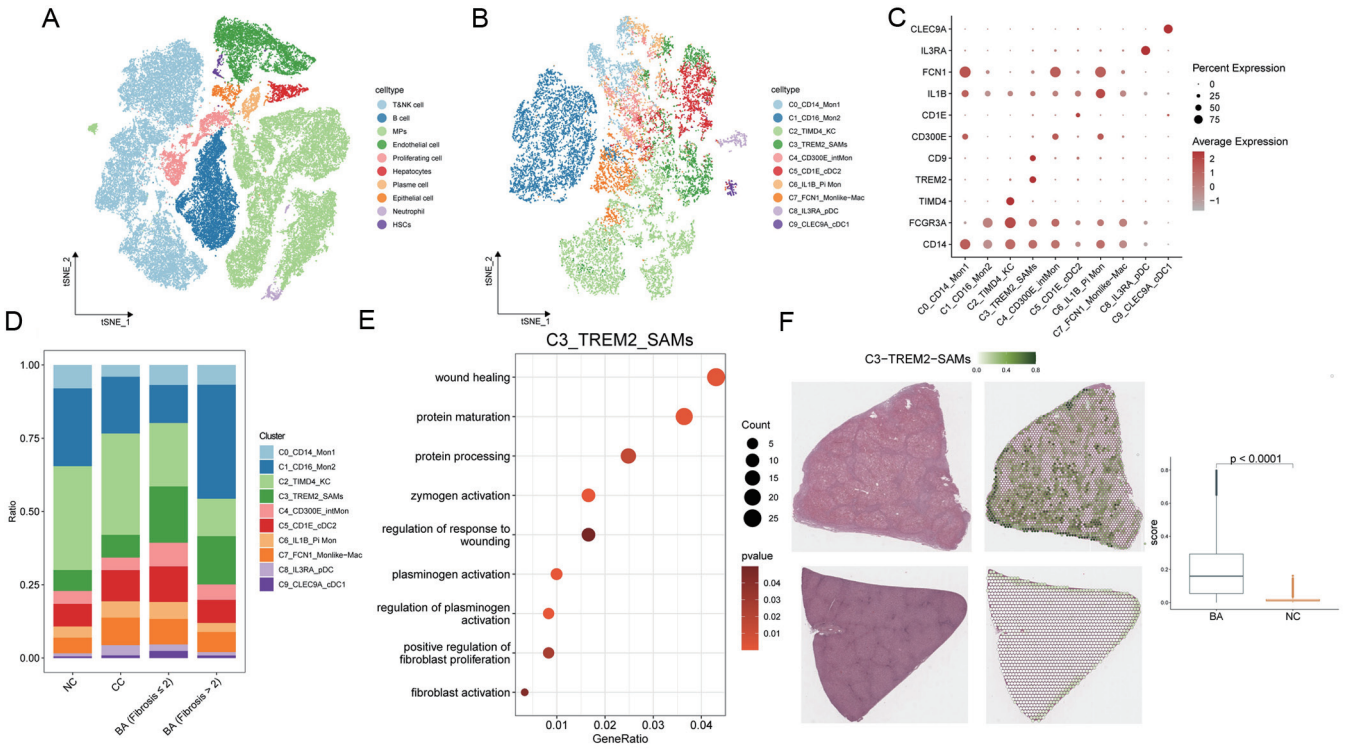

Fig. 1. Single-cell and spatial transcriptomic characterization of scar-associated macrophages in BA. (A) t-SNE plot of major cellular subgroups. (B) t-SNE plot of monocyte–macrophage subgroups. (C) Dot plot of markers for monocyte–macrophage subgroups. (D) Histogram showing the proportions of monocyte–macrophage subgroups. (E) KEGG enrichment analysis of genes highly expressed in SAMs. (F) Spatial localization of SAMs in BA and NC samples. BA, biliary atresia; KEGG, Kyoto Encyclopedia of Genes and Genomes; MPs, monocyte–macrophages; NC, normal control; SAMs, scar-associated macrophages; t-SNE, t-distributed stochastic neighbor embedding.

macrophages, endothelial cells, hepatocytes, epithelial cells, neutrophils, plasma cells, proliferating cells, and HSCs (Fig. 1A–D). SAMs were enriched in BA livers, consistent with our previous findings,[20] and were associated with fibrosis and disease progression severity. Further characterization showed that SAMs highly expressed fibrosis- and inflammation-related genes, including ANXA2, LGALS1, LGALS3, SPP1, and GPNMB (Supplementary Fig. 1A–O, Supplementary Table 9), suggesting potential involvement in inflammatory responses and fibrogenesis. Kyoto Encyclopedia of Genes and Genomes pathway analysis showed that SAM-associated differentially expressed genes were enriched in pathways related to plasminogen activation and fibroblast proliferation and activation (Fig. 1E). Spatial transcriptomics further showed preferential localization and accumulation of SAMs in BA liver tissues compared with NC (Fig. 1F). Collectively, these findings indicate that SAM infiltration is associated with liver fibrosis and BA progression.

PLG–PLGRKT signaling was associated with pro-fibrotic SAM differentiation in BA

To investigate mechanisms underlying SAM generation and differentiation in BA, we analyzed scRNA-seq data by intersecting genes associated with zymogen activation, plasminogen activation, protein processing, and related regulatory pathways and identified five overlapping genes (*ANXA2*, *ENO1*, *CTSZ*, *PLGRKT*, and *PLAUR*) (Fig. 2A). Among these, *PLGRKT* was enriched in the SAM subset (Fig. 2B). Previous studies have shown that PLG binding to *PLGRKT* enhances cell-surface plasminogen activation, leading to localized proteolysis and promoting cell migration and activation of matrix proteases and growth factors.[26] Pseudotemporal trajectory analysis showed that *PLGRKT* expression progressively increased during SAM maturation and was higher in BA than in NC and CC samples (Fig. 2C–D); this pattern was further supported at the tissue level (Fig. 2E). Correlation analysis showed positive associations between *PLGRKT* expression and multiple fibrosis-related genes, including *ANXA2*, *GPNMB*, *LGALS1*, *LGALS3*, *SPP1*, *CD9*, and *TREM2*, with weaker correlations in NC and CC tissues (Fig. 2F and H). Spatial transcriptomics further showed co-localization of *PLGRKT* with SAMs in BA liver tissues (Fig. 2G). Analysis of the Gene Expression Omnibus dataset GSE46960 showed similar positive correlations in BA samples (Supplementary Fig. 2). Collectively, these results suggest that the PLG–*PLGRKT* axis may contribute to SAM differentiation and function during BA progression.

PLGRKT-positive SAMs were associated with fibrosis severity during BA progression

RT-qPCR analysis showed that SAM-associated genes (*CD9*, *TREM2*, *SPP1*, *ANXA2*, *GPNMB*, *LGALS1*, and *LGALS3*) were upregulated in BA liver tissues compared with DC tissues (Supplementary Fig. 3A–B). When BA tissues were stratified by fibrosis stage (F I–II vs F III–IV, METAVIR), these genes were more highly expressed in advanced fibrosis (F III–IV) (Supplementary Fig. 3A–B), indicating an association with fibrosis progression. Similarly, *PLGRKT* mRNA levels were higher in BA tissues and increased with fibrosis stage (Supplementary Fig. 3C). Consistent with the transcriptional data,

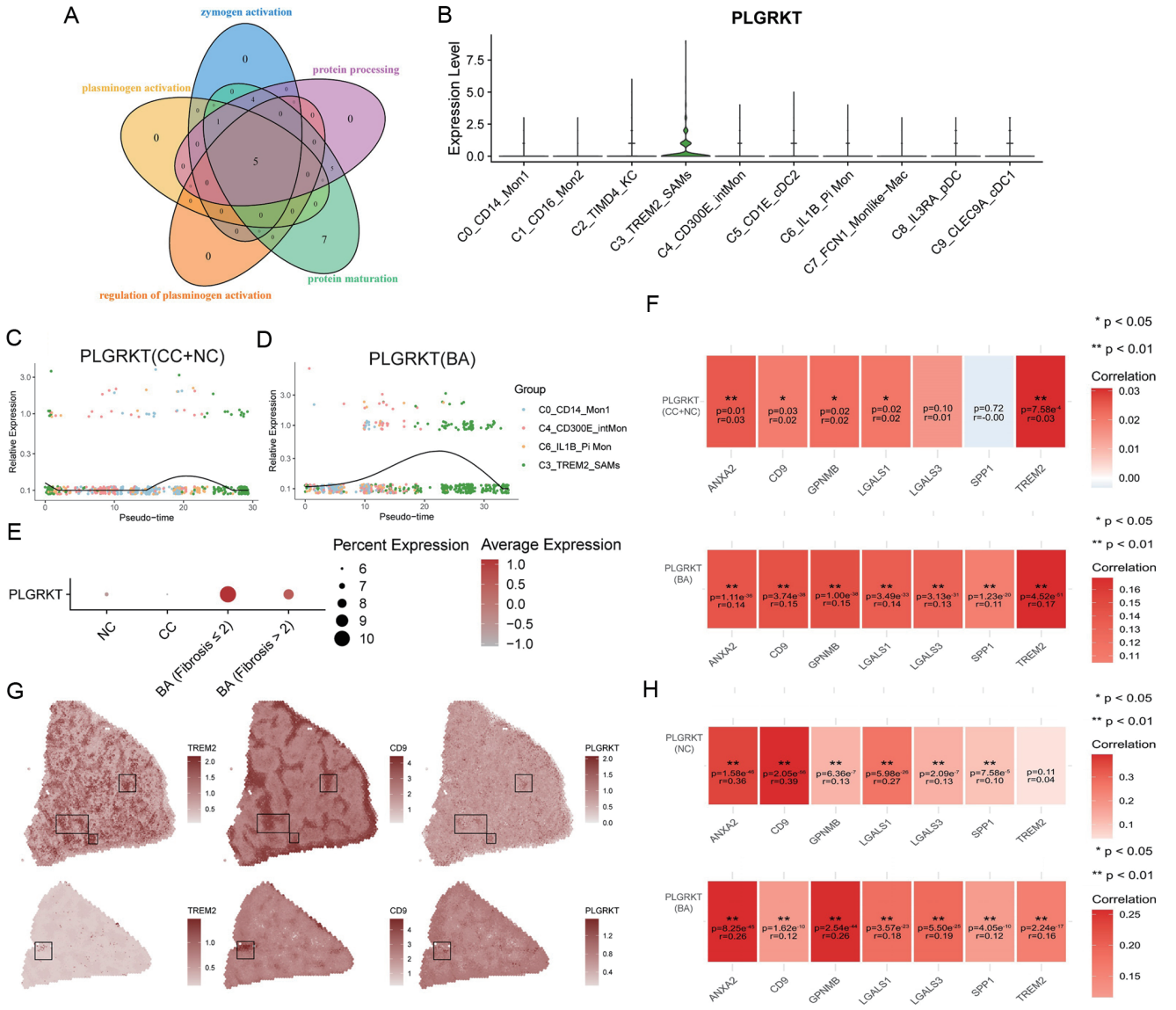

Fig. 2. Single-cell and spatial transcriptomic analysis of *PLGRKT* expression in scar-associated macrophages. (A) Venn diagram showing the intersection of key genes in SAM-enriched signaling pathways. (B) Differential *PLGRKT* expression across SAM subpopulations. (C) Changes in *PLGRKT* expression during SAM differentiation in NC and CC samples. (D) Changes in *PLGRKT* expression during SAM differentiation in BA. (E) *PLGRKT* expression levels in NC, CC, BA (fibrosis ≤ 2), and BA (fibrosis > 2) samples. (F) Correlations between *PLGRKT* and *ANXA2*, *CD9*, *GPNMB*, *LGALS1*, *LGALS3*, *SPP1*, and *TREM2* in scRNA-seq data. (G) Spatial localization of *TREM2*, *CD9*, and *PLGRKT* in liver tissue. (H) Correlations between *PLGRKT* and *ANXA2*, *CD9*, *GPNMB*, *LGALS1*, *LGALS3*, *SPP1*, and *TREM2* in spatial transcriptomic data. BA, biliary atresia; CC, choledochal cyst control; NC, normal control; SAMs, scar-associated macrophages; scRNA-seq, single-cell RNA sequencing.

IHC showed higher CD9, TREM2, and PLGRKT protein expression in BA tissues, with greater expression at stages F III–IV than at F I–II (Fig. 3A and Supplementary Fig. 3D). ELISA showed no significant differences in PLG levels in liver tissue or serum between the BA and DC groups (Supplementary Fig. 3E). Multiplex immunofluorescence showed co-localization of α-SMA, CD68, PLGRKT, CD9, and TREM2 in fibrotic niches, with CD68-positive macrophages co-expressing SAM markers and PLGRKT predominantly adjacent to activated HSCs (Fig. 3B–C and Supplementary Fig. 4A–B), suggesting potential SAM–HSC interactions. Finally, SAM-related functional effectors (α-SMA, ANXA2, GPNMB, LGALS1, LGALS3, and SPP1) were enriched in fibrotic regions and associated with BA progression (Fig. 3D–E and Supplementary Fig. 4C). Overall, these findings indicate that $CD68^+CD9^+TREM2^+PLGRKT^+$ SAMs are associated with fibrosis stage and may interact with HSCs during BA-associated fibrogenesis.

PLG–PLGRKT signaling induced a pro-fibrotic SAM-like phenotype and enhanced HSC collagen deposition in vitro

Because PLG–PLGRKT signaling was associated with SAM generation and enrichment in BA liver tissues, we next examined its functional effects *in vitro*. Human PBMC-derived macrophages were treated with PLG for 6 h to model signals potentially present during tissue injury and remodeling. Flow cytometry showed that PLG treatment increased the proportion of CD9/TREM2-positive SAM-like macrophages (Fig. 4C).

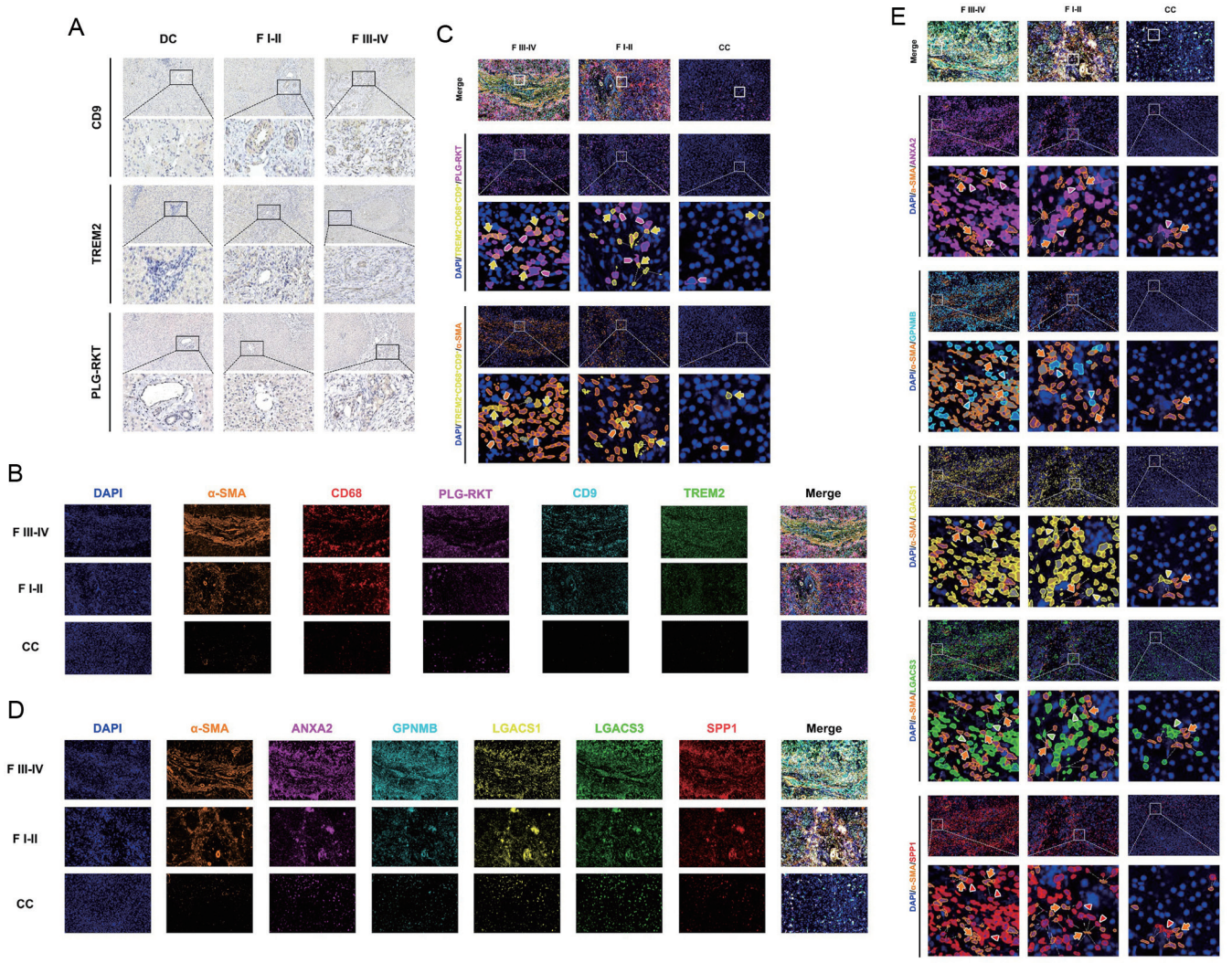

Fig. 3. Immunohistochemical characterization of PLGRKT and SAM-associated markers in liver tissues. (A) Representative immunohistochemical staining for CD9, TREM2, and PLGRKT in liver tissue sections from the study groups. (B) Multiplex immunofluorescence staining of PLGRKT, CD9, TREM2, α-SMA, and CD68 in liver tissues from BA and CC cohorts. DAPI was used for nuclear staining. α-SMA was used as a marker of activated fibroblasts, and CD68 was used as a macrophage marker. (C) Representative multiplex immunofluorescence images showing PLGRKT, α-SMA, and CD68+CD9+TREM2+ cells in liver tissue sections from different study groups. (D–E) Multiplex immunofluorescence staining of SAM-associated proteins (ANXA2, GPNMB, LGALS1, LGALS3, and SPP1) together with α-SMA in liver tissues from BA and CC cohorts. All images were acquired at ×40 magnification. Scale bars, 50 μm.α-SMA, alpha-smooth muscle actin; BA, biliary atresia; CC, choledochal cyst control; DC, disease control; DAPI, 4′,6-diamidino-2-phenylindole; SAMs, scar-associated macrophages.

RT-qPCR further showed increased expression of SAM-associated genes (*TREM2*, *CD9*, *GPNMB*, *LGALS1*, *LGALS3*, *SPP1*, and *ANXA2*) after PLG treatment (Fig. 4D), supporting successful induction of a SAM-like phenotype *in vitro*. Cell–cell communication analysis predicted enhanced signaling interactions between TREM2-positive SAMs and HSCs in BA liver tissues (Fig. 4A and Supplementary Fig. 5), and spatial transcriptomics showed co-localization of *CD9*/*TREM2*-positive SAMs and *ACTA2*-positive HSCs in fibrotic niches (Fig. 4B). To examine indirect SAM–HSC interactions, conditioned medium from PLG-induced SAM-like macrophages (SAM-CM) was applied to LX-2 cells. SAM-CM increased COL1A1 deposition in LX-2 cells (Fig. 4E). We also generated three-dimensional liver organoids by co-culturing THLE-2 liver epithelial cells with LX-2 HSCs. Expression of albumin and PDGFR-β supported successful establishment of the organoid model (Supplementary Fig. 6). SAM-CM also increased COL1A1 deposition in liver organoids (Fig. 4F). Together, these findings indicate that PLG–PLGRKT signaling can promote a SAM-like phenotype *in vitro* and that conditioned medium from these macrophages can increase COL1A1 deposition in HSCs and liver organoids.

PLGRKT silencing attenuated PLG-induced SAM-like features and the pro-fibrotic effects of SAM-conditioned medium in vitro

To determine whether PLG-induced SAM-like differentiation depended on PLGRKT, siRNA targeting PLGRKT was delivered into human PBMC-derived macrophages, and immunofluorescence confirmed PLGRKT knockdown (Fig. 5A). Macrophages with or without PLGRKT knockdown were then treated with PLG. Flow cytometry showed that PLG increased the proportion of CD9/TREM2-positive SAM-like macrophages, whereas PLGRKT silencing reduced this increase (Fig. 5B). Consistent with these findings, RT-qPCR showed that PLG-induced

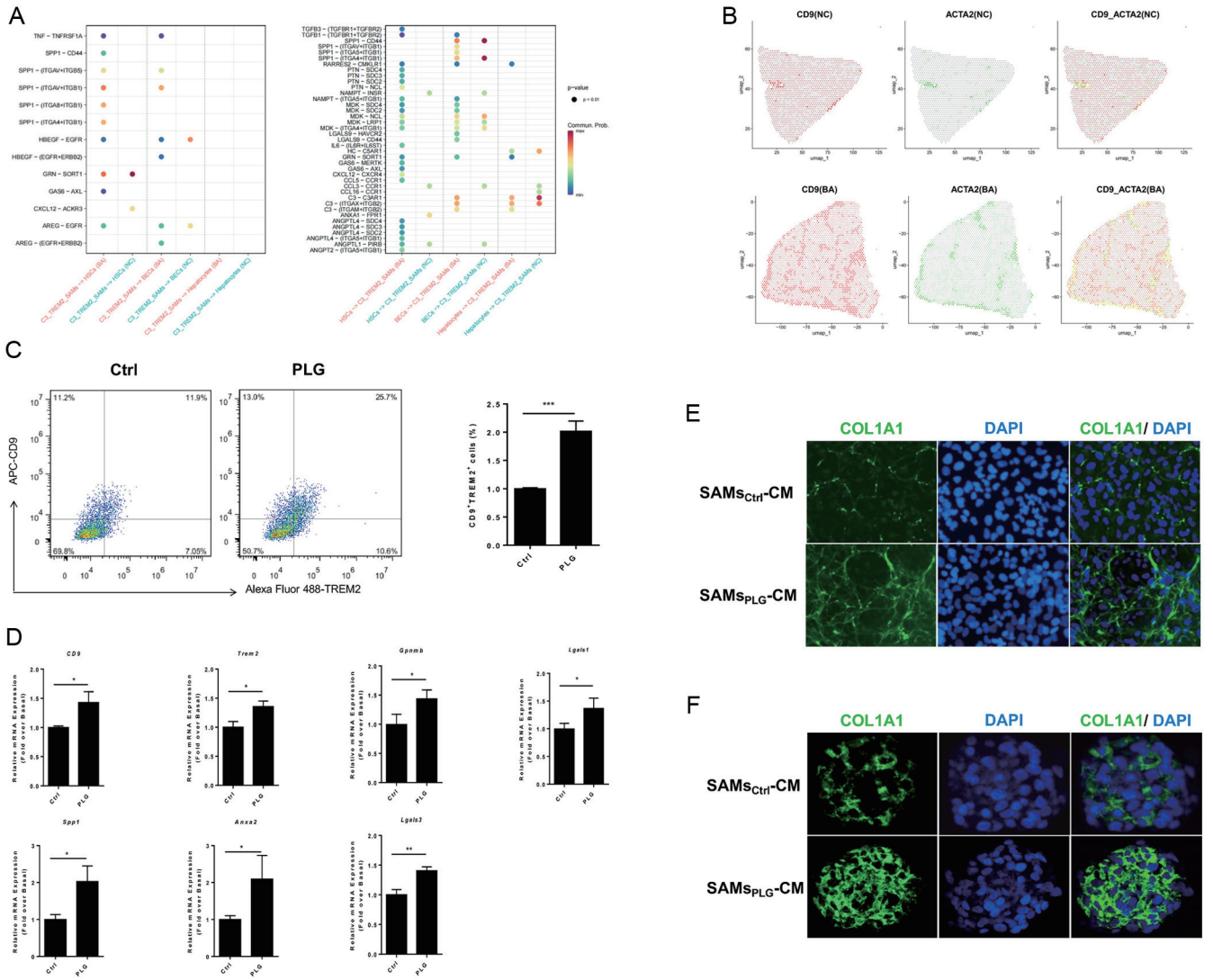

Fig. 4. Characterization of PLG-treated macrophages and their conditioned medium *in vitro*. (A) Cell–cell communication analysis showing predicted interactions between SAMs and HSCs, BECs, and hepatocytes. (B) Spatial co-localization analysis of *CD9* and *ACTA2* expression. Red indicates *CD9* expression, green indicates *ACTA2* expression, and yellow indicates overlapping expression signals. (C) Representative flow cytometry analysis of CD9 and TREM2 expression in macrophages after PLG treatment. (D) RT-qPCR analysis of SAM-associated marker genes (*CD9* and *TREM2*) and other SAM-associated genes (*ANXA2*, *GPNMB*, *LGALS1*, *LGALS3*, and *SPP1*) in macrophages treated with PLG. (E) Representative immunofluorescence staining of COL1A1 in LX-2 cells cultured with conditioned medium from control or PLG-treated macrophages. (F) Representative immunofluorescence staining of COL1A1 in liver organoids cultured with conditioned medium from control or PLG-treated macrophages. Data represent $n = 3$ independent experiments per group. All immunofluorescence images were acquired at ×40 magnification. Scale bars, 50 μm. $^*P < 0.05$, $^{**}P < 0.01$, and $^{***}P < 0.001$. BECs, biliary epithelial cells; HSCs, hepatic stellate cells; PLG, plasminogen; RT-qPCR, reverse transcription quantitative polymerase chain reaction; SAMs, scar-associated macrophages.

increases in SAM-associated genes (*CD9*, *TREM2*, *GPNMB*, *LGALS1*, *ANXA2*, *SPP1*, and *LGALS3*) were attenuated by PLGRKT silencing (Fig. 5C). Conditioned medium from PLGRKT-expressing or PLGRKT-deficient SAM-like macrophages was then applied to LX-2 cells (Fig. 5D) and liver organoids (Fig. 5E). Conditioned medium from PLGRKT-deficient macrophages induced less COL1A1 deposition in both LX-2 cells and liver organoids. These findings support a PLGRKT-dependent role for PLG-induced SAM-like macrophages in modulating HSC fibrogenic responses *in vitro*.

TREM2 antibody-mediated PLGRKT silencing attenuated cholestatic liver fibrosis in BDL mice

We next evaluated the effects of macrophage-targeted PLGRKT silencing *in vivo*. A TREM2 antibody–siRNA conjugate was designed to target TREM2-positive SAMs and exploit TREM2-mediated endocytosis for intracellular delivery of siRNA targeting *Plgrkt* (Fig. 6A). High-performance liquid chromatography showed characteristic peaks for siRNA at 11.223/11.939 min and for the TREM2 antibody at 9.957 min (Supplementary Fig. 7A–B); the conjugate sample showed new peaks at 6.902 and 7.421 min together with residual antibody (9.844 min) and siRNA (11.16/11.792 min) signals, supporting successful coupling (Supplementary Fig. 7C). In vitro uptake assays showed internalization of Cy5-labeled TREM2–siRNA conjugates by RAW264.7 macrophages (Fig. 6B). In vivo distribution experiments further showed co-localization of Cy5-labeled TREM2–siRNA con-

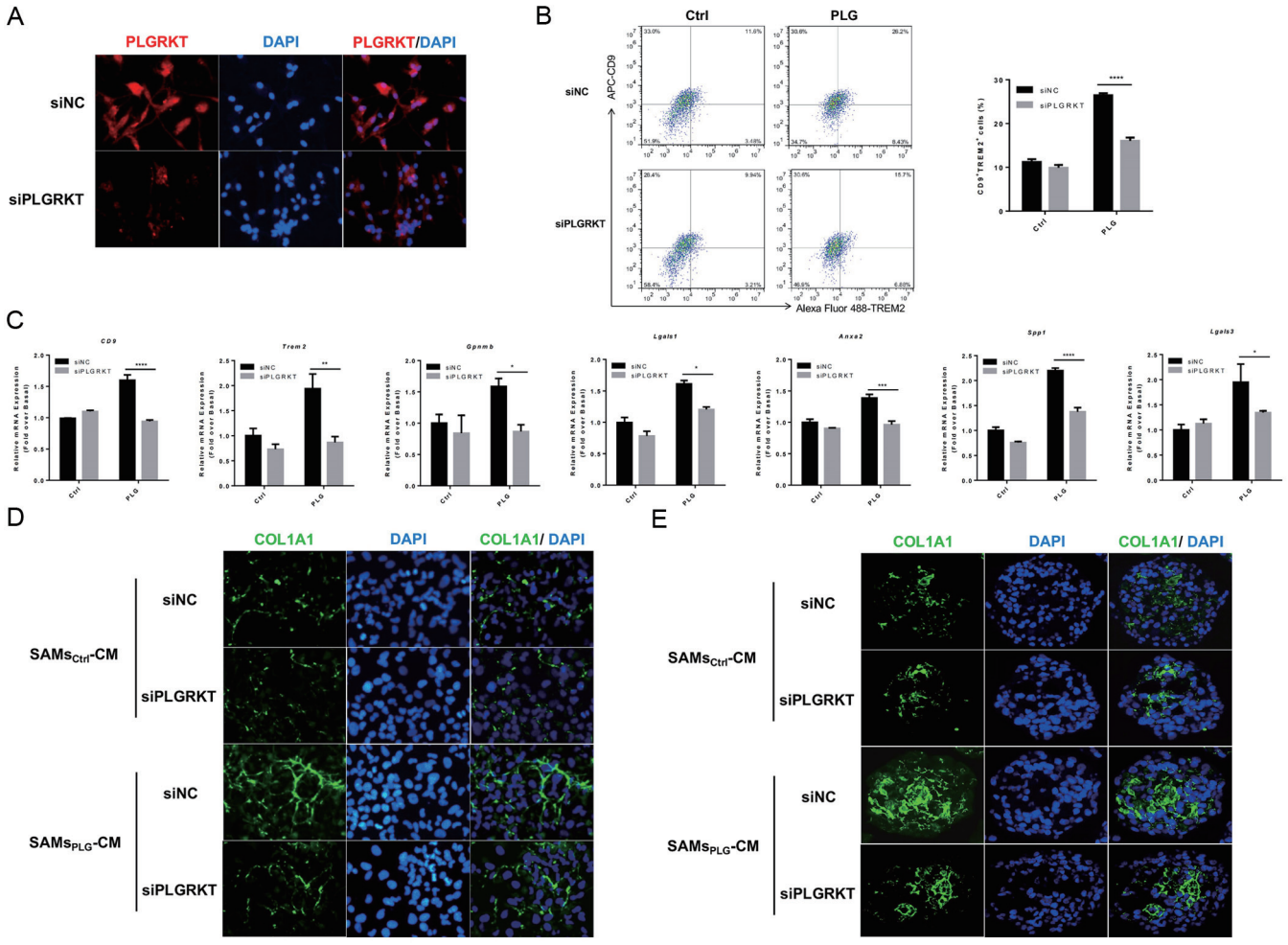

Fig. 5. PLGRKT knockdown in macrophages and downstream effects *in vitro*. (A) Immunofluorescence staining showing PLGRKT expression in macrophages after siRNA transfection. Images were acquired at ×40 magnification. Scale bars, 50 μm. (B) SAM marker expression in macrophages after PLG stimulation with or without siPLGRKT transfection. (C) Expression of SAM-associated genes in macrophages after PLG stimulation with or without siPLGRKT transfection. (D) Collagen deposition in hepatic stellate cells treated with conditioned medium from macrophages after PLG stimulation with or without siPLGRKT transfection. (E) Collagen deposition in liver organoids treated with conditioned medium from macrophages after PLG stimulation with or without siPLGRKT transfection. Data represent $n = 3$ independent experiments per group. *$P < 0.05$, **$P < 0.01$, and ***$P < 0.001$. PLG, plasminogen; SAM, scar-associated macrophage; siRNA, small interfering RNA.

jugates with F4/80-Cy3-labeled macrophages in liver cryosections 2 h after tail-vein injection (Fig. 6C). These pilot studies supported the feasibility of antibody–siRNA-mediated delivery to liver macrophages. To evaluate the potential therapeutic relevance of PLGRKT targeting, we used the BDL mouse model of cholestatic liver injury and fibrosis. Mice subjected to BDL were treated with PLGRKT–TREM2 antibody–siRNA conjugates targeting TREM2-positive SAMs (Fig. 6D). Western blotting showed reduced PLGRKT protein levels in liver tissue after treatment (Fig. 6E). Sirius Red and H&E staining showed attenuation of liver fibrosis (Fig. 6F). Flow cytometry showed that BDL increased the proportion of $CD68^+CD9^+TREM2^+PLGRKT^+$ SAMs in mouse liver tissue, whereas PLGRKT silencing reduced this population (Fig. 6G–H and Supplementary Fig. 8). Serum biochemical analyses further showed that PLGRKT silencing ameliorated BDL-induced liver injury, as reflected by reductions in ALT, AST, ALP, TBA, DBIL, and TBIL levels (Supplementary Fig. 9). RT-qPCR further showed that TREM2-targeted PLGRKT silencing decreased expression of SAM-associated genes (*Trem2*, *Lgals3*, *Anxa2*, *Lgals1*, *Gpnmb*, *Cd9*, and *Spp1*) in BDL mouse liver tissue (Fig. 6I–J). Collectively, these findings show that TREM2-directed PLGRKT silencing reduced SAM accumulation and attenuated liver fibrosis in the BDL model.

Discussion

The rapid progression of liver fibrosis in BA presents a major clinical challenge and highlights the need for effective antifibrotic strategies. Using an integrated approach spanning human omics, tissue validation, and functional models, this study identified the PLGRKT–SAM axis as a potential contributor to BA-associated fibrogenesis. We observed accumulation of monocyte-derived TREM2+CD9+ SAMs within fibrotic niches, consistent with observations in adult human cirrhosis and other fibrotic diseases.[5,9,11,21,23] Validation by RT-qPCR, IHC, and multiplex immunofluorescence showed that SAM abundance was associated with fibrosis severity. SAMs also exhibited a pro-fibrotic transcriptional signature enriched in pathways related to extracellular matrix remodeling and HSC activation.[11,21] Spatial analyses localized these SAMs adjacent to activated HSCs within fibrotic niches, consistent with

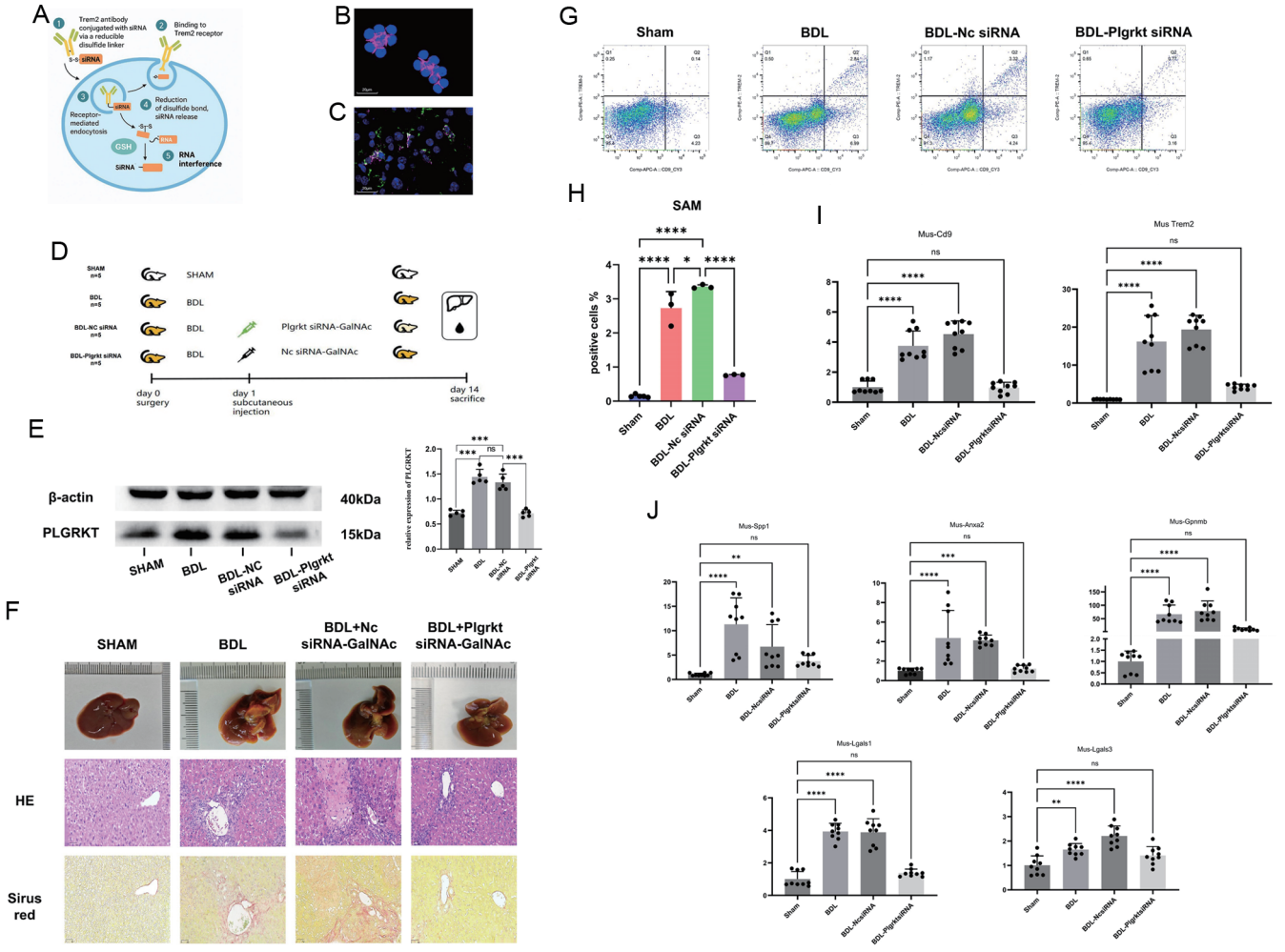

Fig. 6. TREM2 antibody–siRNA conjugate-mediated *Plgrkt* knockdown in SAMs in BDL mice. (A) Schematic illustration of TREM2 antibody–siRNA conjugates used for *Plgrkt* knockdown in SAMs. (B) Uptake of Cy5-labeled TREM2–siRNA conjugates by RAW264.7 macrophages observed by fluorescence microscopy. (C) In vivo localization of Cy5-labeled TREM2–siRNA conjugates with F4/80-Cy3-positive macrophages in liver tissue. (D) Schematic overview of the BDL mouse model and treatment groups. (E) Western blot analysis of Plg-RKT protein levels in liver tissues from different experimental groups. (F) H&E and Sirius Red staining of liver sections from each group. (G) Representative flow cytometry analysis of SAMs (CD45+F4/80+TREM2+CD9+) in liver tissue. (H) Quantification of SAM frequencies across experimental groups. (I) mRNA expression levels of SAM-associated genes (*Trem2* and *Cd9*) measured by RT-qPCR. (J) mRNA expression levels of fibrosis-related genes (*Spp1*, *Anxa2*, *Gpnmb*, *Lgals1*, and *Lgals3*) measured by RT-qPCR. Data represent $n = 5$ per group. $^{*}P < 0.05$, $^{**}P < 0.01$, and $^{***}P < 0.001$. BDL, bile duct ligation; H&E, hematoxylin and eosin; RT-qPCR, reverse transcription quantitative polymerase chain reaction; SAMs, scar-associated macrophages; siRNA, small interfering RNA.

broader models of pro-fibrotic cellular niches across organs and disease states.[9,11,22]

A central finding of this study was the identification of PLGRKT as a regulator associated with the BA SAM phenotype. Although PLGRKT involvement in murine SAM differentiation has been suggested,[12] our data extend these observations to BA. PLGRKT expression was upregulated in BA SAMs, increased along the monocyte-to-SAM differentiation trajectory, correlated with SAM markers and fibrosis stage in patient tissues, and co-localized with SAMs in fibrotic niches. These convergent observations implicate PLGRKT signaling in BA-associated fibrogenesis. In human primary macrophages, PLG stimulation induced a pro-fibrotic SAM-like phenotype that depended on PLGRKT expression. PLGRKT silencing also reduced the ability of SAM-conditioned medium to increase collagen deposition in HSCs in two-dimensional and three-dimensional *in vitro* models.[62–64] Together, these findings support a mechanistic link between macrophage PLGRKT signaling, SAM-like differentiation, and downstream pro-fibrotic activity.

The BDL mouse experiments further support the potential of macrophage-directed PLGRKT targeting. TREM2 is enriched on fibrosis-associated monocyte-derived macrophages and therefore provided a rationale for targeted siRNA delivery. Using TREM2 antibody–siRNA conjugates to inhibit Plgrkt, we observed reduced pro-fibrotic SAM accumulation and attenuated liver fibrosis. A TREM2-blocking antibody directed against TREM2+ macrophages has also been reported to reduce lung fibrosis *in vivo*, providing precedent for macrophage-directed TREM2 targeting.[65]

From a translational perspective, these findings address an important unmet need in BA management: the absence of pharmacological anti-fibrotic therapy capable of preventing progressive fibrogenesis after Kasai portoenterostomy. The present results identify PLGRKT as a candidate target in BA-associated SAMs and provide preclinical proof of concept for TREM2 antibody–siRNA-mediated macrophage-directed delivery. However, the specificity, safety, pharmacokinetics,

and off-target effects of this approach require further evaluation before clinical translation. The association between SAM abundance and fibrosis stage also warrants further investigation of these cells as potential biomarkers for risk stratification or longitudinal monitoring. In addition, the liver organoid–macrophage co-culture system used here may provide an ex vivo platform for preclinical evaluation of PLGRKT-targeted interventions. Overall, the PLGRKT–SAM axis merits further investigation as a mechanism-based target for macrophage-directed anti-fibrotic strategies in BA and potentially other pediatric fibrotic cholangiopathies.

Several limitations should be considered. First, adult liver cell lines were used to establish the cellular and organoid models. Because BA primarily affects neonates and infants, these adult immortalized cell lines may not fully reproduce the developmental and immune features of the neonatal BA biliary microenvironment. Future studies should therefore validate the findings using patient-derived or induced pluripotent stem cell-derived cholangiocyte or hepatocyte organoids. Second, the BDL mouse model reproduces obstructive cholestasis and fibrosis but does not capture the full pathogenesis of BA, including potential viral or immune-mediated bile-duct injury. Rhesus rotavirus-induced BA models may provide a complementary system for future studies. Third, the downstream mechanisms through which PLGRKT regulates fibrogenesis were not defined. Future work incorporating PLGRKT gain- and loss-of-function models and RNA sequencing may help identify downstream signaling pathways and candidate targets.

Conclusions

By integrating human single-cell and spatial omics, patient-tissue validation, *in vitro* functional assays, and an *in vivo* preclinical model, this study identified the PLGRKT–SAM axis as a potential contributor to BA-associated liver fibrosis. Monocyte-derived $TREM2^{+}CD9^{+}$ SAMs accumulated in fibrotic niches, and PLGRKT expression increased with SAM differentiation and fibrosis severity. Targeted PLGRKT silencing reduced SAM accumulation and attenuated cholestatic fibrosis in the BDL mouse model. These findings support PLGRKT as a candidate mediator and potential therapeutic target that warrants further validation in BA-specific models.

Supporting information

Supplementary material for this article is available at https://doi.org/10.14218/JCTH.2026.00278.

Acknowledgments

Artificial intelligence (AI)-assisted image generation was used to prepare the graphical abstract. The graphical abstract was initially generated using ChatGPT (OpenAI, GPT-5.5) based on author-designed scientific content and was subsequently revised, verified, and finalized by the authors.

Funding

This study was supported by the Tianshan Talent Training Program (Grant No. 2023TSYCJC0052), the Natural Science Foundation Projects of Xinjiang Uygur Autonomous Region (Grant No. 2024D01A28), and the Tianjin Applied Basic Research Project Planning Project (Grant No. 22JCZDJC00290). The funding agencies had no role in data collection, analysis, or interpretation; manuscript drafting or revision; or the decision to submit the manuscript for publication.

Conflict of interest

The authors have no conflict of interests related to this publication.

Author contributions

Study design and data analysis (XL, TL, SL); experiments (XL, YC, XX, YlZ, RS); data collection (TL, SL, JL, YrZ); drafting and revision of the manuscript (XL, TL, SL, QY, YM); figure revision (QY, TL, YM); critical revision of the manuscript (AA). All authors contributed to the article and approved the final version.

Ethical statement

The human tissue study was conducted in accordance with the Declaration of Helsinki (as revised in 2024), and approved by the Ethics Committee of Urumqi Children's Hospital (K2024-04). Written informed consent was obtained from the legal guardian of each patient. Animal experiments were additionally approved by the relevant ethics committee (approval no. GENINK-20250194). All animals received humane care.

Data sharing statement

The GSE46960 dataset has been deposited in a public, open-access data repository. The datasets generated and analyzed in this study are available in the OMIX database (https://ngdc.cncb.ac.cn/omix/) under accession number OMIX008911. Further information is available from the corresponding author upon request.

References

[1] Hartley JL, Davenport M, Kelly DA. Biliary atresia. Lancet 2009;374(9702):1704–1713. doi:10.1016/S0140-6736(09)60946-6, PMID:19914515.
[2] Bezerra JA, Wells RG, Mack CL, Karpen SJ, Hoofnagle JH, Doo E, *et al*. Biliary Atresia: Clinical and Research Challenges for the Twenty-First Century. Hepatology 2018;68(3):1163–1173. doi:10.1002/hep.29905, PMID:29604222.
[3] McKiernan PJ. Neonatal cholestasis. Semin Neonatol 2002;7(2):153–165. doi:10.1053/siny.2002.0103, PMID:12208100.
[4] Wang P, Zhang HY, Yang J, Zhu T, Wu X, Yi B, *et al*. Severity assessment to guide empiric antibiotic therapy for cholangitis in children after Kasai portoenterostomy: a multicenter prospective randomized control trial in China. Int J Surg 2023;109(12):4009–4017. doi:10.1097/JS9.0000000000000682, PMID:37678274.
[5] Kisseleva T, Brenner D. Molecular and cellular mechanisms of liver fibrosis and its regression. Nat Rev Gastroenterol Hepatol 2021;18(3):151–166. doi:10.1038/s41575-020-00372-7, PMID:33128017.
[6] Friedman SL. Hepatic stellate cells: protean, multifunctional, and enigmatic cells of the liver. Physiol Rev 2008;88(1):125–172. doi:10.1152/physrev.00013.2007, PMID:18195085.
[7] Tacke F, Zimmermann HW. Macrophage heterogeneity in liver injury and fibrosis. J Hepatol 2014;60(5):1090–1096. doi:10.1016/j.jhep.2013.12.025, PMID:24412603.
[8] Vonderlin J, Chavakis T, Sieweke M, Tacke F. The Multifaceted Roles of Macrophages in NAFLD Pathogenesis. Cell Mol Gastroenterol Hepatol 2023;15(6):1311–1324. doi:10.1016/j.jcmgh.2023.03.002, PMID:36907380.
[9] Bhattacharya M, Ramachandran P. Immunology of human fibrosis. Nat Immunol 2023;24(9):1423–1433. doi:10.1038/s41590-023-01551-9, PMID:37474654.
[10] Jiang YZ, Zhao XY, Zhou GP, Wei L, Qu W, Zeng ZG, *et al*. Impact of immunosuppression level on liver allograft fibrosis after pediatric liver transplantation: a retrospective cohort study. Int J Surg 2023;109(11):3450–3458. doi:10.1097/JS9.0000000000000631, PMID:37578449.
[11] Ramachandran P, Dobie R, Wilson-Kanamori JR, Dora EF, Henderson BEP, Luu NT, *et al*. Resolving the fibrotic niche of human liver cirrhosis at single-cell level. Nature 2019;575(7783):512–518. doi:10.1038/s41586-019-1631-3, PMID:31597160.
[12] Yang Y, Li W, Liu C, Liu J, Yang L, Yue W, *et al*. Single-cell RNA seq identifies Plg-R(KT)-PLG as signals inducing phenotypic transformation of scar-associated macrophage in liver fibrosis. Biochim Biophys Acta Mol Basis Dis 2023;1869(6):166754. doi:10.1016/j.bbadis.2023.166754, PMID:372

07518.
[13] Lee KJ, An S, Kim MY, Kim SM, Jeong WI, Ko HJ, *et al*. Hepatic TREM2(+) macrophages express matrix metalloproteinases to control fibrotic scar formation. Immunol Cell Biol 2023;101(3):216–230. doi:10.1111/imcb.12616, PMID:36529983.
[14] Fabre T, Barron AMS, Christensen SM, Asano S, Bound K, Lech MP, *et al*. Identification of a broadly fibrogenic macrophage subset induced by type 3 inflammation. Sci Immunol 2023;8(82):eadd8945. doi:10.1126/sciimmunol.add8945, PMID:37027478.
[15] Morse C, Tabib T, Sembrat J, Buschur KL, Bittar HT, Valenzi E, *et al*. Proliferating SPP1/MERTK-expressing macrophages in idiopathic pulmonary fibrosis. Eur Respir J 2019;54(2):1802441. doi:10.1183/13993003.02441-2018, PMID:31221805.
[16] Aran D, Looney AP, Liu L, Wu E, Fong V, Hsu A, *et al*. Reference-based analysis of lung single-cell sequencing reveals a transitional profibrotic macrophage. Nat Immunol 2019;20(2):163–172. doi:10.1038/s41590-018-0276-y, PMID:30643263.
[17] Kuppe C, Ibrahim MM, Kranz J, Zhang X, Ziegler S, Perales-Patón J, *et al*. Decoding myofibroblast origins in human kidney fibrosis. Nature 2021;589(7841):281–286. doi:10.1038/s41586-020-2941-1, PMID:33176333.
[18] Hoeft K, Schaefer GJL, Kim H, Schumacher D, Bleckwehl T, Long Q, *et al*. Platelet-instructed SPP1(+) macrophages drive myofibroblast activation in fibrosis in a CXCL4-dependent manner. Cell Rep 2023;42(2):112131. doi:10.1016/j.celrep.2023.112131, PMID:36807143.
[19] Amrute JM, Luo X, Penna V, Yang S, Yamawaki T, Hayat S, *et al*. Targeting immune-fibroblast cell communication in heart failure. Nature 2024;635(8038):423–433. doi:10.1038/s41586-024-08008-5, PMID:39443792.
[20] Li X, Li T, Liu S, Zhao Y, Chen Y, Abudureyimu A, *et al*. Scar-associated macrophages and biliary epithelial cells interaction exacerbates hepatic fibrosis in biliary atresia. Pediatr Res 2026;99(1):362–374. doi:10.1038/s41390-025-04100-2, PMID:40383871.
[21] Lee J, Kim CM, Cha JH, Park JY, Yu YS, Wang HJ, *et al*. Multiplexed Digital Spatial Protein Profiling Reveals Distinct Phenotypes of Mononuclear Phagocytes in Livers with Advanced Fibrosis. Cells 2022;11(21):3387. doi:10.3390/cells11213387, PMID:36359782.
[22] Ye C, Zhu J, Wang J, Chen D, Meng L, Zhan Y, *et al*. Single-cell and spatial transcriptomics reveal the fibrosis-related immune landscape of biliary atresia. Clin Transl Med 2022;12(11):e1070. doi:10.1002/ctm2.1070, PMID:36333281.
[23] Henlon Y, Panir K, McIntyre I, Hogg C, Dhami P, Cuff AO, *et al*. Single-cell analysis identifies distinct macrophage phenotypes associated with prodisease and proresolving functions in the endometriotic niche. Proc Natl Acad Sci U S A 2024;121(38):e2405474121. doi:10.1073/pnas.2405474121, PMID:39255000.
[24] Wang J, Xu Y, Chen Z, Liang J, Lin Z, Liang H, *et al*. Liver Immune Profiling Reveals Pathogenesis and Therapeutics for Biliary Atresia. Cell 2020;183(7):1867–1883.e26. doi:10.1016/j.cell.2020.10.048, PMID:33248023.
[25] Guilliams M, Bonnardel J, Haest B, Vanderborght B, Wagner C, Remmerie A, *et al*. Spatial proteogenomics reveals distinct and evolutionarily conserved hepatic macrophage niches. Cell 2022;185(2):379–396.e38. doi:10.1016/j.cell.2021.12.018, PMID:35021063.
[26] Miles LA, Plow EF, Waisman DM, Parmer RJ. Plasminogen receptors. J Biomed Biotechnol 2012;2012:130735. doi:10.1155/2012/130735, PMID:23226936.
[27] Andronicos NM, Chen EI, Baik N, Bai H, Parmer CM, Kiosses WB, *et al*. Proteomics-based discovery of a novel, structurally unique, and developmentally regulated plasminogen receptor, Plg-RKT, a major regulator of cell surface plasminogen activation. Blood 2010;115(7):1319–1330. doi:10.1182/blood-2008-11-188938, PMID:19897580.
[28] Vago JP, Sugimoto MA, Lima KM, Negreiros-Lima GL, Baik N, Teixeira MM, *et al*. Plasminogen and the Plasminogen Receptor, Plg-R(KT), Regulate Macrophage Phenotypic, and Functional Changes. Front Immunol 2019;10:1458. doi:10.3389/fimmu.2019.01458, PMID:31316511.
[29] Bessho K, Mourya R, Shivakumar P, Walters S, Magee JC, Rao M, *et al*. Gene expression signature for biliary atresia and a role for interleukin-8 in pathogenesis of experimental disease. Hepatology 2014;60(1):211–223. doi:10.1002/hep.27045, PMID:24493287.
[30] Bedossa P, Poynard T. An algorithm for the grading of activity in chronic hepatitis C. The METAVIR Cooperative Study Group. Hepatology 1996;24(2):289–293. doi:10.1002/hep.510240201, PMID:8690394.
[31] Butler A, Hoffman P, Smibert P, Papalexi E, Satija R. Integrating single-cell transcriptomic data across different conditions, technologies, and species. Nat Biotechnol 2018;36(5):411–420. doi:10.1038/nbt.4096, PMID:29608179.
[32] McGinnis CS, Murrow LM, Gartner ZJ. DoubletFinder: Doublet Detection in Single-Cell RNA Sequencing Data Using Artificial Nearest Neighbors. Cell Syst 2019;8(4):329–337.e4. doi:10.1016/j.cels.2019.03.003, PMID:30954475.
[33] Hafemeister C, Satija R. Normalization and variance stabilization of single-cell RNA-seq data using regularized negative binomial regression. Genome Biol 2019;20(1):296. doi:10.1186/s13059-019-1874-1, PMID:31870423.
[34] Ghosh D. Incorporating the empirical null hypothesis into the Benjamini-Hochberg procedure. Stat Appl Genet Mol Biol 2012;11(4). doi:10.1515/1544-6115.1735, PMID:22850065.
[35] Yu G, Wang LG, Han Y, He QY. clusterProfiler: an R package for comparing biological themes among gene clusters. OMICS 2012;16(5):284–287. doi:10.1089/omi.2011.0118, PMID:22455463.
[36] Qiu X, Mao Q, Tang Y, Wang L, Chawla R, Pliner HA, *et al*. Reversed graph embedding resolves complex single-cell trajectories. Nat Methods 2017;14(10):979–982. doi:10.1038/nmeth.4402, PMID:28825705.
[37] Jin S, Guerrero-Juarez CF, Zhang L, Chang I, Ramos R, Kuan CH, *et al*. Inference and analysis of cell-cell communication using CellChat. Nat Commun 2021;12(1):1088. doi:10.1038/s41467-021-21246-9, PMID:33597522.
[38] Ståhl PL, Salmén F, Vickovic S, Lundmark A, Navarro JF, Magnusson J, *et al*. Visualization and analysis of gene expression in tissue sections by spatial transcriptomics. Science 2016;353(6294):78–82. doi:10.1126/science.aaf2403, PMID:27365449.
[39] Fischer AH, Jacobson KA, Rose J, Zeller R. Hematoxylin and eosin staining of tissue and cell sections. CSH Protoc 2008;2008:pdb.prot4986. doi:10.1101/pdb.prot4986, PMID:21356829.
[40] Zhao E, Stone MR, Ren X, Guenthoer J, Smythe KS, Pulliam T, *et al*. Spatial transcriptomics at subspot resolution with BayesSpace. Nat Biotechnol 2021;39(11):1375–1384. doi:10.1038/s41587-021-00935-2, PMID:34083791.
[41] Aibar S, González-Blas CB, Moerman T, Huynh-Thu VA, Imrichova H, Hulselmans G, *et al*. SCENIC: single-cell regulatory network inference and clustering. Nat Methods 2017;14(11):1083–1086. doi:10.1038/nmeth.4463, PMID:28991892.
[42] Ramos-Vara JA. Technical aspects of immunohistochemistry. Vet Pathol 2005;42(4):405–426. doi:10.1354/vp.42-4-405, PMID:16006601.
[43] Schneider CA, Rasband WS, Eliceiri KW. NIH Image to ImageJ: 25 years of image analysis. Nat Methods 2012;9(7):671–675. doi:10.1038/nmeth.2089, PMID:22930834.
[44] Junqueira LC, Bignolas G, Brentani RR. Picrosirius staining plus polarization microscopy, a specific method for collagen detection in tissue sections. Histochem J 1979;11(4):447–455. doi:10.1007/BF01002772, PMID:91593.
[45] Stack EC, Wang C, Roman KA, Hoyt CC. Multiplexed immunohistochemistry, imaging, and quantitation: a review, with an assessment of Tyramide signal amplification, multispectral imaging and multiplex analysis. Methods 2014;70(1):46–58. doi:10.1016/j.ymeth.2014.08.016, PMID:25242720.
[46] Desjardins P, Conklin D. NanoDrop microvolume quantitation of nucleic acids. J Vis Exp 2010;45:e2565. doi:10.3791/2565, PMID:21189466.
[47] Livak KJ, Schmittgen TD. Analysis of relative gene expression data using real-time quantitative PCR and the 2(-Delta Delta C(T)) Method. Methods 2001;25(4):402–408. doi:10.1006/meth.2001.1262, PMID:11846609.
[48] Sugo T, Terada M, Oikawa T, Miyata K, Nishimura S, Kenjo E, *et al*. Development of antibody-siRNA conjugate targeted to cardiac and skeletal muscles. J Control Release 2016;237:1–13. doi:10.1016/j.jconrel.2016.06.036, PMID:27369865.
[49] Tag CG, Sauer-Lehnen S, Weiskirchen S, Borkham-Kamphorst E, Tolba RH, Tacke F, *et al*. Bile duct ligation in mice: induction of inflammatory liver injury and fibrosis by obstructive cholestasis. J Vis Exp 2015;96:e52438. doi:10.3791/52438, PMID:25741630.
[50] Fuss IJ, Kanof ME, Smith PD, Zola H. Isolation of whole mononuclear cells from peripheral blood and cord blood. Curr Protoc Immunol 2009;85:7.1.1–7.1.8. doi:10.1002/0471142735.im0701s85, PMID:19347849.
[51] Martinez FO, Gordon S, Locati M, Mantovani A. Transcriptional profiling of the human monocyte-to-macrophage differentiation and polarization: new molecules and patterns of gene expression. J Immunol 2006;177(10):7303–7311. doi:10.4049/jimmunol.177.10.7303, PMID:17082649.
[52] Elbashir SM, Lendeckel W, Tuschl T. RNA interference is mediated by 21- and 22-nucleotide RNAs. Genes Dev 2001;15(2):188–200. doi:10.1101/gad.862301, PMID:11157775.
[53] Pfeifer AM, Cole KE, Smoot DT, Weston A, Groopman JD, Shields PG, *et al*. Simian virus 40 large tumor antigen-immortalized normal human liver epithelial cells express hepatocyte characteristics and metabolize chemical carcinogens. Proc Natl Acad Sci U S A 1993;90(11):5123–5127. doi:10.1073/pnas.90.11.5123, PMID:7685115.
[54] Yoon Y, Gong SC, Kim MY, Baik SK, Hong JE, Rhee KJ, *et al*. Generation of Fibrotic Liver Organoids Using Hepatocytes, Primary Liver Sinusoidal Endothelial Cells, Hepatic Stellate Cells, and Macrophages. Cells 2023;12(21):2514. doi:10.3390/cells12212514, PMID:37947592.
[55] Igarashi R, Oda M, Okada R, Yano T, Takahashi S, Pastuhov S, *et al*. Generation of human adult hepatocyte organoids with metabolic functions. Nature 2025;641(8065):1248–1257. doi:10.1038/s41586-025-08861-y, PMID:40240606.
[56] Coll M, Perea L, Boon R, Leite SB, Vallverdú J, Mannaerts I, *et al*. Generation of Hepatic Stellate Cells from Human Pluripotent Stem Cells Enables In Vitro Modeling of Liver Fibrosis. Cell Stem Cell 2018;23(1):101–113.e7. doi:10.1016/j.stem.2018.05.027, PMID:30049452.
[57] Pradere JP, Kluwe J, De Minicis S, Jiao JJ, Gwak GY, Dapito DH, *et al*. Hepatic macrophages but not dendritic cells contribute to liver fibrosis by promoting the survival of activated hepatic stellate cells in mice. Hepatology 2013;58(4):1461–1473. doi:10.1002/hep.26429, PMID:23553591.
[58] Maecker HT, Trotter J. Flow cytometry controls, instrument setup, and the determination of positivity. Cytometry A 2006;69(9):1037–1042. doi:10.1002/cyto.a.20333, PMID:16888771.
[59] Mederacke I, Dapito DH, Affò S, Uchinami H, Schwabe RF. High-yield and high-purity isolation of hepatic stellate cells from normal and fibrotic mouse livers. Nat Protoc 2015;10(2):305–315. doi:10.1038/nprot.2015.017, PMID:25612230.
[60] Towbin H, Staehelin T, Gordon J. Electrophoretic transfer of proteins from polyacrylamide gels to nitrocellulose sheets: procedure and some applications. Proc Natl Acad Sci U S A 1979;76(9):4350–4354. doi:10.1073/pnas.76.9.4350, PMID:388439.
[61] Wai CT, Greenson JK, Fontana RJ, Kalbfleisch JD, Marrero JA, Conjeevaram HS, *et al*. A simple noninvasive index can predict both significant

fibrosis and cirrhosis in patients with chronic hepatitis C. Hepatology 2003;38(2):518–526. doi:10.1053/jhep.2003.50346, PMID:12883497.
[62] Liu F, Lui VCH, Wu Z, Blakeley PD, Tang CSM, Tam PKH, *et al*. Animal and organoid models to elucidate the anti-fibrotic effect of steroid on biliary atresia. Pediatr Surg Int 2024;40(1):214. doi:10.1007/s00383-024-05798-7, PMID:39102048.
[63] Amarachintha SP, Mourya R, Ayabe H, Yang L, Luo Z, Li X, *et al*. Biliary organoids uncover delayed epithelial development and barrier function in biliary atresia. Hepatology 2022;75(1):89–103. doi:10.1002/hep.32107, PMID:34392560.
[64] Chusilp S, Lee C, Li B, Lee D, Yamoto M, Ganji N, *et al*. A novel model of injured liver ductal organoids to investigate cholangiocyte apoptosis with relevance to biliary atresia. Pediatr Surg Int 2020;36(12):1471–1479. doi:10.1007/s00383-020-04765-2, PMID:33084932.
[65] Cui H, Banerjee S, Xie N, Hussain M, Jaiswal A, Liu H, *et al*. TREM2 promotes lung fibrosis via controlling alveolar macrophage survival and profibrotic activity. Nat Commun 2025;16(1):1761. doi:10.1038/s41467-025-57024-0, PMID:39971937.